Marine Chemistry 173 (2015) 67–77

Contents lists available at ScienceDirect

Marine Chemistry

journal homepage: www.elsevier.com/locate/marchem

Modeling organic iron-binding ligands in a three-dimensional biogeochemical ocean model

Christoph Völker [a,*,1], Alessandro Tagliabue [b,1]

[a] Alfred-Wegener-Institut Helmholtz-Zentrum für Polar-und Meeresforschung, Am Handelshafen 12, Bremerhaven, Germany
[b] School of Environmental Sciences, University of Liverpool, 4 Brownlow Street, Liverpool L69 3GP, United Kingdom

ARTICLE INFO

Article history:
Received 13 June 2014
Received in revised form 6 November 2014
Accepted 15 November 2014
Available online 20 November 2014

Keywords:
Iron
Organic complexation
Dissolved organic carbon
Model

ABSTRACT

Most dissolved iron in the ocean is bound to organic molecules with strong conditional stability constants, known as ligands that are found at concentrations ranging from 0.2 to more than 10 nmol L^{-1}. In this work we report the first mechanistic description of ligand dynamics in two three-dimensional models of ocean biogeochemistry and circulation. The model for ligands is based on the concept that ligands are produced both from organic matter remineralization and phytoplankton processes, and that they are lost through bacterial and photochemical degradation, as well as aggregation and to some extent in the process of phytoplankton uptake of ligand-bound iron. A comparison with a compilation of in-situ measurements shows that the model is able to reproduce some large-scale features of the observations, such as a decrease in ligand concentrations along the conveyor belt circulation in the deep ocean, lower surface and subsurface values in the Southern Ocean, or higher values in the mesopelagic than in the abyssal ocean.

Modeling ligands prognostically (as opposed to assuming a uniform ligand concentration) leads to a more nutrient-like profile of iron that is more in accordance with data. It however, also leads to higher surface concentrations of dissolved iron and negative excess ligand L_* in some ocean regions. This is probably an indication that with more realistic and higher ligand concentrations near the surface, as opposed to the traditionally chosen low uniform concentration, iron modelers will have to re-evaluate their assumption of low scavenging rates for iron. Given their sensitivity to environmental conditions, spatio-temporal variations in ligand concentrations have the potential to impact primary production via changes in iron limitation.

1. Introduction

Due to its biological necessity, iron (Fe) is a key resource for marine phytoplankton (Geider and La Roche, 1994) and is considered as the limiting nutrient in a number of oceanic regions (Moore et al., 2013). These include the classic high nutrient low chlorophyll regions of the Southern Ocean (de Baar et al., 1995), equatorial Pacific (Martin et al., 1994), sub-Arctic Pacific (Martin and Fitzwater, 1988) and to a lesser extent seasonally in the North Atlantic (Nielsdóttir et al., 2009). Moreover, Fe can also regulate the rates of nitrogen fixation by diazotrophs in tropical regions (Schlosser et al., 2014). Accordingly most ocean general circulation and biogeochemistry models (OGCBMs) that seek to represent ocean biogeochemical cycling, including those concerned with climate change, represent Fe.

The process of organic complexation by molecules known as ligands is a key feature of the ocean Fe cycle. In oxygenated seawater equilibrium free Fe concentrations are extremely low (Liu and Millero, 2002) and appreciable dissolved Fe is only present due to complexation by organic molecules called ligands (Gledhill and Buck, 2012). Generally speaking, ligands act to buffer the dissolved Fe concentration by restricting its loss via scavenging and precipitation. Due to their role in governing the residence time of Fe in the ocean, varying the assumptions regarding the concentrations of ligands has significant impacts on atmospheric CO_2 (Tagliabue et al., 2014). The electrochemical methods used to determine oceanic ligand concentrations often discriminate between two ligand classes, a strong and weak ligand pool (Rue and Bruland, 1995).

Surface water ligand concentrations are variable (from 0.2 to >10 nmol L^{-1}) and their sources reflect the combination of a number of different production pathways (see: Gledhill and Buck (2012) and references therein). For example, the Fe stressed biota can 'actively' produce strong binding ligands (so-called L1 ligands with a conditional stability constant similar to known bacterial siderophores) to complex Fe (Wilhelm and Trick, 1994; Gledhill et al., 2004). However, while recent work has identified siderophore-like groups in seawater (Macrellis et al., 2001; Mawji et al., 2008), their concentrations are very low relative to the total ligand concentration. But there are also other pathways that may explain the observed covariance of ligands with phytoplankton

* Corresponding author.
E-mail addresses: christoph.voelker@awi.de (C. Völker), a.tagliabue@liverpool.ac.uk (A. Tagliabue).
[1] Both authors contributed equally to this manuscript.

http://dx.doi.org/10.1016/j.marchem.2014.11.008

(Gerringa et al., 2006): Weaker binding ligands can be produced by 'passive' processes linked to exudates (such as exopolysaccharides, Hassler et al., 2011) or the cellular debris arising from mortality and heterotrophic activity (e.g., the chlorophyll breakdown product phaeophytin or hemes and other porphyrins, Hutchins et al. (1999)), similar to dissolved organic carbon (DOC) cycling. Indeed, ligand concentrations have increased following enhanced biological activity in Fe addition experiments (e.g., Boye et al., 2005) and in response to increased grazing rates in shipboard experiments (Sato et al., 2007). Further support for 'passive' production similar to DOC comes from Mediterranean mesocosm observations of a strong covariance between ligands and DOC (Wagener et al., 2008).

Away from the surface, vertical profiles of ligands from the Southern (e.g., Ibisanmi et al., 2011) and Atlantic Oceans (e.g. Mohamed et al., 2011) show elevated concentrations of ligands at mid water depth coincident with macronutrient maxima, implying a remineralisation source (Wu et al., 2001). This is supported by the first measurements of ligand production rates from particle degradation during incubation experiments (Boyd et al., 2010) and in situ correlations between nitrate (NO_3^-) or phosphate (PO_4^{3-}) and Fe solubility (indicative of ligand concentrations, e.g. Schlosser and Croot (2009)). In the abyssal ocean, ligand concentrations appear to decrease along the 'conveyor belt' from the Atlantic, to Southern and Pacific Oceans (e.g. Thuróczy et al., 2011; Mohamed et al., 2011; Kondo et al., 2012), again similar to DOC (Hansell et al., 2012). This may indicate that ligands contain a 'background' refractory pool that might be relatively long lived and terrestrially derived humic substances (e.g. Laglera and van den Berg, 2009).

Differential surface and deep-water production pathways were recently conceptually linked (Hunter and Boyd, 2007). This view emphasizes surface production connected to phytoplankton processes and subsurface production from organic matter remineralisation. This conceptual model has led to some initial modeling in one-dimension (Ye et al., 2009); one result of that modeling was that ligand lifetimes in the deep ocean must be longer than a decade, prompting the need for three-dimensional modeling.

While OGCBMs consider the complexation of Fe by ligands with varying degrees of complexities, they still all assume constant ligand concentrations (Parekh et al., 2005; Aumont and Bopp, 2006; Moore and Braucher, 2008). Some recent works have considered empirical representations of ligand concentrations linked to DOC or oxygen consumption, but these do not explicitly represent the key processes (Misumi et al., 2013; Tagliabue and Völker, 2011). Given their role in regulating the dissolved Fe concentration, it is likely that the ability of OGCBMs to reproduce the growing inventory of Fe observations will be regulated by their omission of ligand dynamics. For example, uniform ligand concentrations lead to a correspondingly uniform deep ocean dissolved Fe concentration in models, which is in discord with the latest observational constraints (Tagliabue et al., 2012).

In this work we report the first mechanistic description of ligand dynamics from two three-dimensional models of ocean circulation and biogeochemistry. We compare the results with a compilation of in-situ measurements, discuss how a nonconstant ligand distribution affects the distribution of iron, and test the limits of our understanding with a series of sensitivity experiments.

2. Model description

Given that open-ocean measurements are still sparse, and — partly due to different analytical windows of the electrochemical determinations — one does not always have the information on whether there are really two distinct ligand classes, we have decided to neglect the distinction between strong and weak ligand classes for the time being and model one generic ligand pool. Implementing a prognostic ligand therefore means describing sources and sinks for only one additional biogeochemical tracer, ligand concentration, that is integrated forward in time alongside other biogeochemical tracers.

2.1. Sources and sinks of ligands

One may distinguish between two main pathways for the production of iron-binding ligands (Hunter and Boyd, 2007): One is the degradation of organic macromolecules, e.g. porphyrins or ferritin, by bacteria, releasing fragments that have a capacity to bind iron (Boyd et al., 2010) (and possibly other metals). The other is the direct production of ligands by living organisms, probably mostly by prokaryotes. These sources of ligand are best described coupled to other processes that are present in the model (e.g. carbon remineralization and DOC production). The initial assumptions made here are that the remineralization source of ligands is proportional to the remineralization of dead particulate organic carbon, with a constant ratio $r_{L:C}$ between the release of ligand and that of dissolved carbon, $S_{rem} = r_{L:C} f_T k_{rem} POC$, where f_T is the temperature dependence of detritus degradation, k_{rem} is the detritus degradation rate at reference temperature, and POC is the organic carbon in detritus.

Ligand production by living organisms is described in the present model as proportional to the release of non-refractory dissolved organic carbon, again with a constant ligand:carbon ratio $r_{L:DOC}$, i.e. $S_{DOC} = r_{L:DOC} S_{DOC}$, where S_{DOC} is the source term for dissolved organic carbon from living organisms. Note that thus we do not make the production explicitly dependent on iron stress. In REcoM, however, DOC production is coupled to carbon overconsumption under nutrient stress (Schartau et al., 2007), so one might argue that limitation is taken into account indirectly. In PISCES this is not the case.

Four loss processes for organic ligands are represented in the model. The first is bacterial degradation. While freshly produced siderophores are likely to be degraded quickly due to their small size and simple functional groups, the weaker ligands found in the deep ocean probably have a much longer degradation timescale as seen for DOC (Hansell et al., 2012). We attempt to take this continuum of ligands into account without explicitly resolving several distinct ligand pools by making the timescale of degradation τ_d a simple function of ligand concentration as

$$\tau_d = \max(\tau_{min}, \tau_{max} \exp(-aL)) \quad (1)$$

where L is the concentration of ligand and a is a scaling factor, that we set to 2 L nmol^{-1}. The total rate of degradation is then $R_{deg} = (f_T/\tau)L$, where f_T is the temperature dependency of bacterial processes, which in our models is given by an Arrhenius function with a $Q_{10} \approx 2$. The net result of Eq. (1) is to make ligands at high concentrations degrade much faster than ligands at low concentration.

The second loss process is photochemical degradation. Barbeau et al. (2003) have shown that some organic ligands are photoreactive, while others are not. In the model we parameterize the process simply as a degradation rate which is proportional to light, times the total ligand concentration $R_{phot} = k_{ph} I L$, where I is the downwelling irradiance. More complicated formulations are certainly conceivable, but are difficult to implement in a global model at this stage.

The third process we include as a loss of ligands is uptake of organically complexed Fe by phytoplankton. While not all forms of complexed Fe are equally bioavailable to all groups of phytoplankton (Hutchins et al., 1999), in general, ligand-bound iron can be taken up (e.g. Maldonado and Price, 1999), using a range of different uptake mechanisms (Maldonado and Price, 2001; Shaked et al., 2005; Boukhalfa and Crumbliss, 2002). Several of these mechanisms are likely to result in a net loss of complexing capacity. In the model we thus describe the loss of ligands through uptake as $R_{upt} = p_{upt} R_{Fe}$, where p_{upt} is a probability that iron uptake destroys a ligand molecule and R_{Fe} is the uptake of iron by phytoplankton.

Finally, part of the ligands is certainly colloidal (Cullen et al., 2006) and can aggregate with sinking particles. In the model this process is described as $R_{col} = p_{col} \lambda L$, where p_{col} is the fraction of ligands that

undergoes aggregation and L is the total ligand concentration. λ is an aggregation rate, which we calculate from the concentrations of dissolved and particulate organic carbon and aggregation kernels for shear and Brownian motion (Jackson and Burd, 1998). At the moment, we assume that aggregated ligand is lost from the system completely, unlike for iron, where PISCES allows for re-dissolution of particulate iron.

2.2. Model parameters

The ligand model as described above contains several parameters that must be chosen, namely $r_{L:C}$, k_{phot}, τ_{max}, τ_{min}, p_{upt} and p_{col}. While direct measurements of each are unavailable at present, we can make first order approximations of their likely range from previous work (the sensitivity to each will be explored in additional model experiments).

Concerning first the ratio of ligand to carbon $r_{L:C}$, the seasonal variations in ligand and DOC concentrations at the DYFAMED site in the Mediterranean by Wagener et al. (2008) show a good ligand:DOC correlation with a slope of $\approx 10^{-4}$ mol L mol^{-1} C. A second constraint comes from a linear correlation between iron solubility (a proxy for organic ligands) and regenerated phosphate in the Mauritanian upwelling (Schlosser and Croot, 2009) with a slope of $\approx 10^{-3}$ mol L mol^{-1} P. Using the Redfield ratio of 106 mol mol^{-1} for C:P this translates into a ligand:C range $10^{-4} < r_{L:C} < 10^{-5}$ mol mol^{-1}. The shipboard incubation experiments with particles sampled in the water column at a polar and a subantarctic site south of Australia by Boyd et al. (2010) found a release of ligands and of iron in a ratio of ≈5 mol mol^{-1}. Assuming a typical Fe:C ratio in biogenic particles of $\approx 5 - 20 \cdot 10^{-6}$ mol mol^{-1}, this translates into a ligand:carbon ratio of $2.5 - 10 \cdot 10^{-5}$ mol mol^{-1}, within the range estimated above.

Hansell et al. (2012) gives a range of degradation time-scales for dissolved organic carbon from 1.5 years for semi-labile DOC to 16,000 years for refractory DOC. We assume that the ligands that we are modeling are part of the continuum between semi-labile and more refractory DOC with a minimum degradation time-scale τ_{min} of one year and a maximum time-scale τ_{max} of 1000 years (at a reference temperature of 0 °C).

There are so far only a few experiments that allow the determination of the rate constant for photochemical ligand degradation. We have estimated our rate k_{phot} from Powell and Wilson-Finelli (2003), but study the sensitivity to this parameter further in Section 5. This holds also for the fraction of ligands that undergoes aggregation p_{col}, which we assume to be 0.5 in the reference experiment. We assume that uptake always destroys ligands, i.e. that the fraction of ligands that is on average destroyed when phytoplankton cells take up iron p_{upt} is one.

2.3. Model runs

The way that iron is modeled in different ocean biogeochemical models differs considerably, and it is conceivable that this has as large an effect on the modeled ligand distributions as varying the ligand model parameters. To obtain an idea on the sensitivity of our model results to the underlying biogeochemical model, we therefore present here results obtained with two different global biogeochemical models, with the same formulation for ligand dynamics. The two models are PISCES (Aumont and Bopp, 2006; Tagliabue et al., 2014), and REcoM (Hauck et al., 2013); both have been described elsewhere, but without a prognostic ligand. Both represent phytoplankton by two functional groups, diatoms and nondiatoms, and also have compartments for zooplankton and dead organic matter (detritus). REcoM is slightly simpler in that it resolves only one zooplankton and detritus class, while PISCES has two. On the other hand, REcoM allows for decoupling of the carbon and nitrogen cycling by allowing deviations of the cellular stoichiometry from the classical Redfield ratio.

For a full description of the model we refer the reader to Tagliabue et al. (2014) and Hauck et al. (2013); instead we focus here on the added component organic ligand, whose dynamics are described equally in both models.

With each of the models we performed one standard model run, which was the outcome of a number of previous sensitivity studies. The ligand model parameters belonging to these standard runs (Table 1) are identical, except that REcoM uses half the ligand to carbon ratio that PISCES does; this was deemed necessary to produce realistic surface ligand concentrations, and — as we will discuss in the next section — can be traced back to a different emphasis placed on POC remineralization and DOC excretion in the two models.

To elucidate some of the dependencies of model outcomes to some uncertain parameter values, we also did a series of sensitivity experiments with one of the models, REcoM, only. In these experiments the parameters for ligand:carbon ratio $r_{L:C}$ (runs L2C1 and L2C2), for photochemistry k_{phot} (runs PHOT1 and PHOT2), and for the fraction of ligands undergoing aggregation p_{col} (runs COL1 and COL2) are varied. Parameter values for these runs are also documented in Table 1.

Both models were integrated for 2000 years with annually repeating atmospheric forcing, starting from a uniform ligand concentration (0.6 nmol L^{-1} in the case of PISCES, 1.0 nmol L^{-1} for REcoM). Shown distributions are annual averages from the last model year. Sensitivity experiments were integrated for 1000 years.

A difference between the models is that REcoM assumes the ligands to have a uniform conditional stability constant with $pK_{Fe'L} = 11$, while the stability constant in PISCES is set to vary with temperature, following $pK_{Fe'L} = 17.27 - 1565.7/T_K$ where T_K is absolute temperature. This leads to a $pK_{Fe'L}$ of 11.5 at 0 °C and 11.9 at 20 °C. The net effect of this temperature dependency is that iron is scavenged slightly more easily in colder waters than in warmer waters.

2.4. Ligand data compilation

To be able to evaluate the model, we compiled a data set of in-situ observations from the published literature. In doing so, we did not take into account that measurement methods for ligands still differ strongly in their methodology, e.g. through the application of different competing ligands in the electrochemical titrations, and consequently different analytical windows for ligand stability constants. We certainly do not see our data compilation as the last word on a ligand database, rather as a first attempt to obtain at least a semi-quantitative data set for evaluation. The complete list of papers and data sets that we included can be found in the supplement to this paper.

3. Ligand distribution and comparison to observations

The compilation of in-situ observations (shown as filled circles in Figs. 1 and 2) shows that a uniform constant value evidently is not supported by the data, and that, moreover, a constant value of 0.6 or 1 nmol L^{-1} is an underestimate of the true ligand concentration.

The distribution of ligands as it is produced by PISCES (model run LIGA, Fig. 1) clearly does a better job than the assumption of a constant value. A few characteristic features are: Surface concentrations are

Table 1
Parameter value settings for the two 'standard' model runs LIGA and LIGB, and the sensitivity runs considered further in Section 5.

Name	$r_{L:C}$ 10^{-3} mol mol^{-1}	p_{upt} –	p_{col} –	k_{phot} 10^{-4} W^{-1} m^2 d^{-1}	τ_{min} yr	τ_{max} yr	Model
LIGA	0.1	1.0	0.5	1.0	1	1000	PISCES
LIGB	0.05	1.0	0.5	1.0	1	1000	REcoM
L2C1	0.07	1.0	0.5	1.0	1	1000	REcoM
L2C2	0.1	1.0	0.5	1.0	1	1000	REcoM
PHOT1	0.1	1.0	0.5	1.86	1	1000	REcoM
PHOT2	0.1	1.0	0.5	5.0	1	1000	REcoM
COL1	0.1	1.0	0.0	1.0	1	1000	REcoM
COL2	0.1	1.0	1.0	1.0	1	1000	REcoM

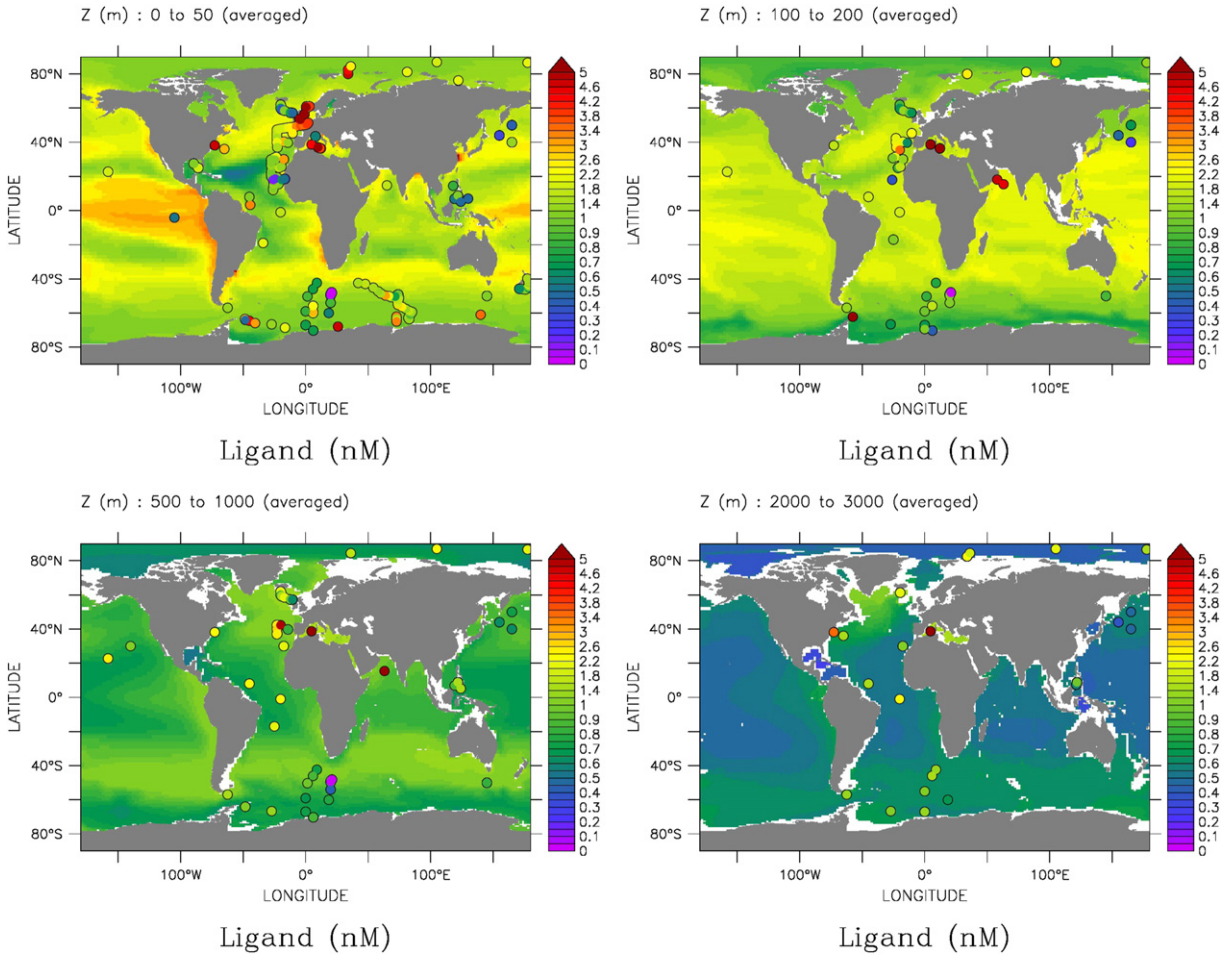

Fig. 1. Ligand distribution after 2000 years in run LIGA. The compiled in-situ measurements are also shown as symbols in the same color coding.

highest in upwelling regions and over some shelves, somewhat elevated in the subpolar regions, and decrease towards higher latitudes and the centers of subtropical gyres. Below the euphotic zone, concentrations are more homogenous, but still present the same general pattern. In the mesopelagic, values become generally lower, but remain the highest below ocean regions that are characterized by a stronger biological carbon pump. In the deep ocean the influence of lateral advection becomes apparent in elevated concentrations around Antarctica and the North Atlantic, while concentrations in the oldest water masses in the North Pacific are significantly lower.

One may argue that several of the model predictions, such as the lower surface ligand concentrations in the Southern Ocean and the higher ligand concentrations there in the deep, are also seen in our collection of in-situ observations. There are other features where model and observations do not match so well, e.g. in the equatorial upwelling in the Pacific (albeit against one data point), where the model overestimates ligands, or the deep Atlantic, where modeled ligand concentrations are slightly too low. Other predictions, such as the lower concentrations of ligands that typify the centers of the subtropical gyres are difficult to assess at the moment from the available data. Overall, model bias with respect to our compilation of ligand data is reduced from -0.89 nmol L^{-1} to -0.19 nmol L^{-1} in the LIGA model, compared to the assumption of a constant ligand concentration of 0.6 nmol L^{-1}. Root mean square error (RMSE) also decreases slightly in model LIGA, from 2.2 nmol L^{-1} to 2.0 nmol L^{-1}.

The distribution of ligands in the REcoM model (model run LIGB, Fig. 2) is qualitatively similar but also shows some characteristic differences: There is less tendency for elevated ligand concentrations in upwelling regions, which improves the fit to the single data point in the equatorial upwelling in the Pacific, and a reduced tendency for lower ligand concentrations in the Atlantic subtropical gyres. Compared to the assumption of a constant ligand concentration of 1.0 nmol L^{-1}, bias is reduced from -0.47 nmol L^{-1} to -0.10 nmol L^{-1} in model run LIGB, and root mean square error (RMSE) decreases from 2.1 nmol L^{-1} to 1.4 nmol L^{-1}. Overall, Atlantic and Indian Ocean surface values are generally higher in REcoM than seen in PISCES, with slightly lower values for the Pacific. Below the euphotic zone, the patterns are quite similar in the models with a decrease from the subtropical regions to the higher latitudes, especially the Southern Ocean. In the deep ocean, the distribution with REcoM shows some more structure than in PISCES, with a stronger east–west gradient especially in the North Atlantic (this likely reflects differences in the overturning strength between the models).

PISCES and REcoM show inter-model differences in their ability to reproduce the observations, which is underpinned by how each model represents the sources and sinks of ligands. For example, PISCES seems to better match observations in the surface, while REcoM does better in the ocean interior (Figs. 1 and 2). When the globally integrated sources and sinks of ligands are compared (Table 2), we see that PISCES and REcoM place similar weight on bacterial degradation and photochemistry, but differ in terms of the two ligand source terms and the coagulation loss. REcoM produces slightly more ligands than PISCES via DOC-based production (S_{DOC}, 8.1 versus $7.2 \cdot 10^{10}$ mol yr^{-1}, Table 2), despite the 2-fold lower production ratio in REcoM (Table 1). This greater emphasis on DOC production in REcoM thus explains the higher surface ligand concentrations compared to PISCES. On the other hand, PISCES places much more emphasis on subsurface production, with production from organic matter remineralization (S_{REM}) of $22.6 \cdot 10^{10}$ mol yr^{-1}, compared to $8.8 \cdot 10^{10}$ mol yr^{-1} in REcoM (Table 2). While this difference is more

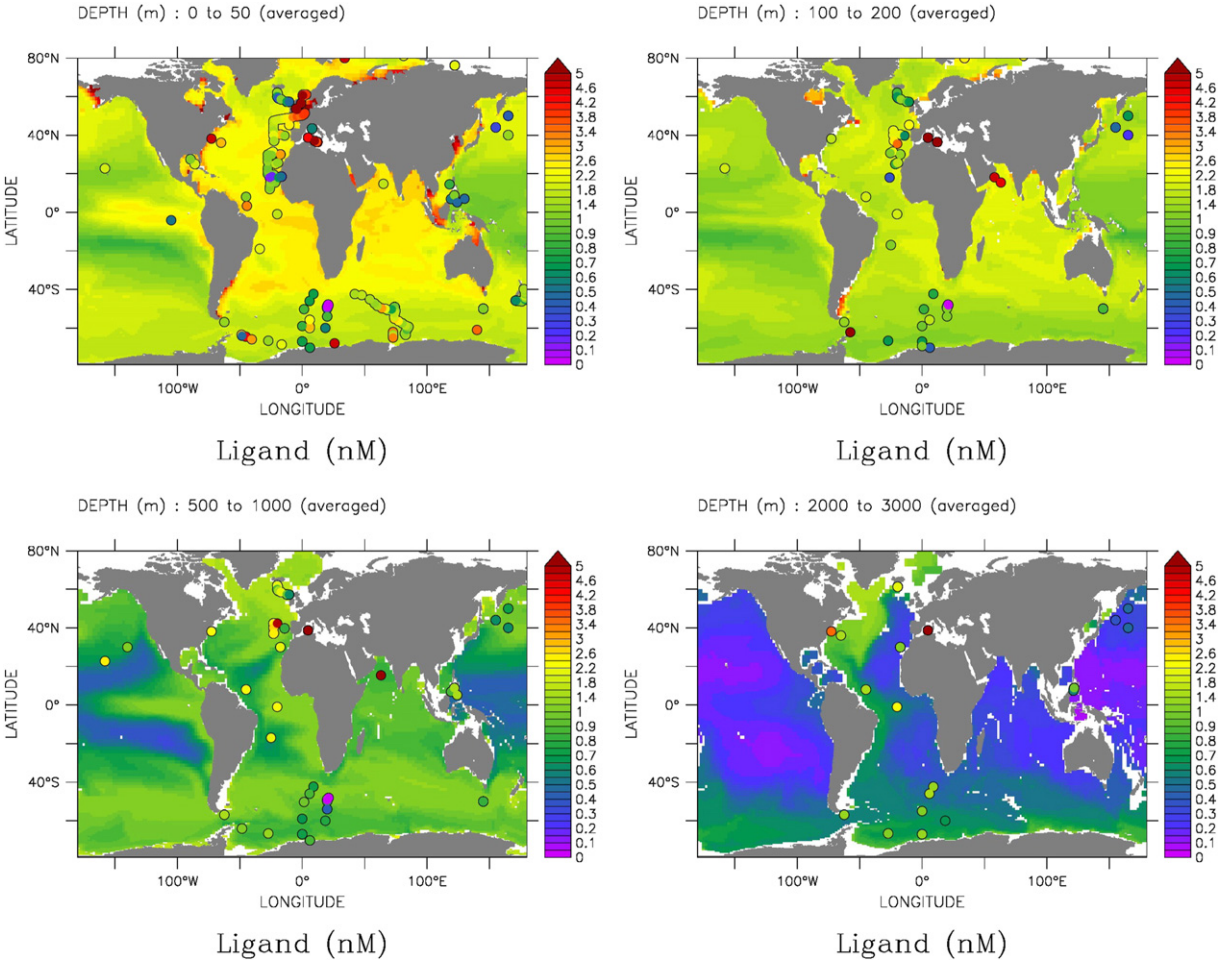

Fig. 2. Ligand distribution after 2000 years in model run LIGB. Symbols in the same color coding show our compilation of in situ-measurements.

than would be expected from the greater production ratio in PISCES it is offset by some degree by much greater loss of ligands via coagulation (R_{col}) than in REcoM (18.8 and $5.6 \cdot 10^{10}$ mol yr^{-1}, Table 2). The balance between S_{REM} and R_{col} in PISCES means that the subsurface ligand concentrations are only slightly higher in PISCES, relative to REcoM (Figs. 1 and 2).

4. Changes in the iron distribution with prognostic ligands

The concentration of ligands affects the equilibrium distribution of iron between inorganic forms (mainly hydroxides for ferrous iron) and iron bound to the ligands. The high particle reactivity of the inorganic forms drives scavenging, a main loss process for dissolved iron. It is therefore expected that a spatio-temporal variation of ligand concentration has consequences for the distribution of iron in the ocean.

This is indeed what is found: A comparison of the (globally averaged) vertical profiles (Fig. 3) of iron in model runs with variable organic ligands with runs where the ligand concentration was kept fixed at a constant value throughout the ocean shows a general tendency of iron concentrations to increase in the upper part of the ocean and to decrease somewhat in the deep part. A notable feature is that both models now show a more nutrient-like profile for dissolved iron than with constant ligand, with an intermediate maximum around 500 m depth, near the depth of the oxygen minimum. This is closer to observations than in the case with constant ligands, where deep iron tends to be too homogeneous compared to observations (Tagliabue et al., 2012).

It is interesting to note that, both with prognostic and with constant ligands, the average iron profile differs in several respects between the two models: PISCES has a local maximum near the surface, and for constant ligand has a slight secondary maximum at 3000 m depth. Both features are absent in REcoM. This can be traced back to a different treatment of iron sources in the two models: PISCES has a comparatively strong sedimentary source of iron which is strongest on shallow shelves, and includes hydrothermal inputs of iron (Tagliabue et al., 2014), while REcoM has only a weak sediment source and neglects hydrothermalism altogether. Given this difference, it is encouraging that in both models, qualitatively, the introduction of prognostic ligands leads to a more nutrient-like iron profile.

Of direct importance for biological productivity are of course mainly the changes in iron concentration through prognostic ligands in the euphotic zone. Fig. 4 shows how near-surface (0–50 m) iron changes in the model runs with prognostic ligands, compared to a model run with constant ligand. Although details of the patterns differ slightly between the two models, the general picture is robust, namely that dissolved iron increases most in the Atlantic and Indian Ocean, while only small changes are seen in the Southern Ocean and the Pacific.

Table 2
Globally integrated source and sink terms for the organic ligand in the two 'standard' model runs. Here S_{rem} is the source from remineralization from organic particles, S_{DOC} is the source connected with excretion of DOC, R_{rem} is the bacterial degradation, R_{phot} is photochemical degradation, R_{upt} is the loss of ligands connected to iron uptake, and R_{col} is the loss through colloid aggregation. All numbers are given in 10^{10} mol L $year^{-1}$.

Name	S_{rem}	S_{DOC}	R_{rem}	R_{phot}	R_{upt}	R_{col}
LIGA	22.6	7.2	−5.0	−2.2	−6.7	−18.8
LIGB	8.8	8.1	−6.4	−3.1	−2.5	−5.6

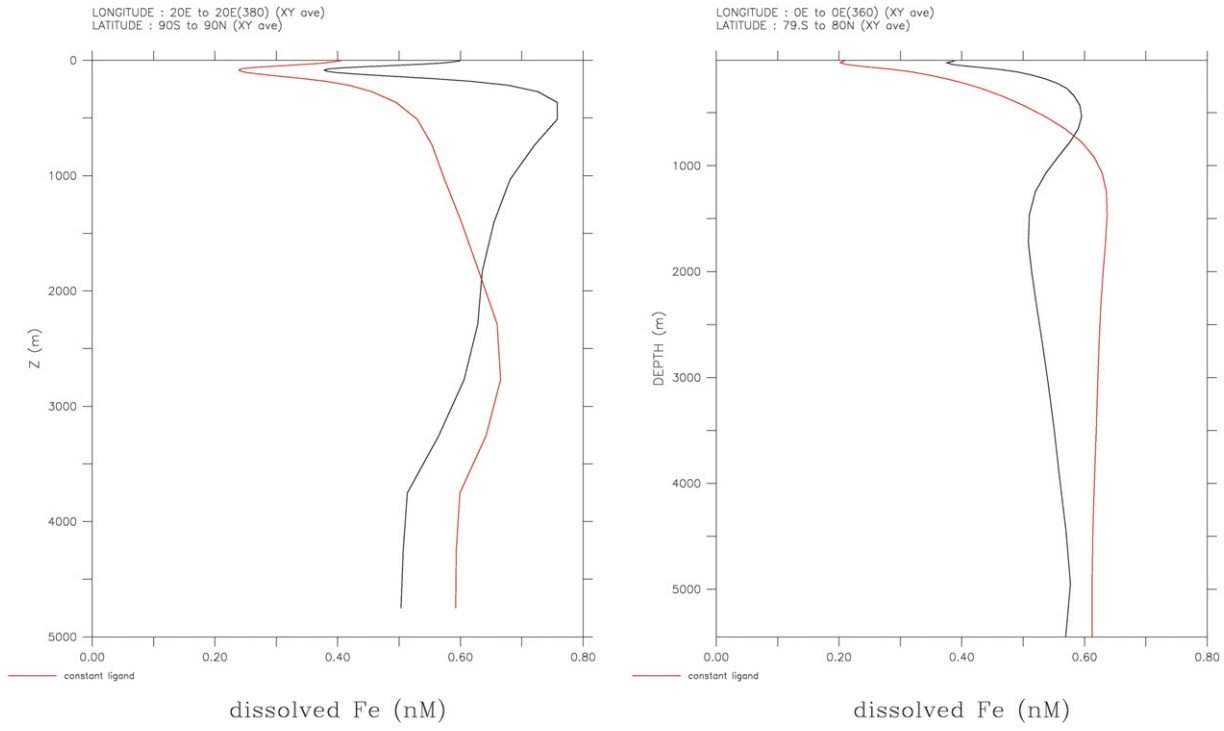

Fig. 3. Globally averaged iron profiles with and without variable ligands in model run LIGA (left), and in run LIGB (right) after 2000 years.

This pattern reflects the fact that in the latter regions, production in the models tends to be iron-limited, so that here biological uptake is the main loss process for iron, not scavenging. An increase in ligands therefore does not lead to an increased lifetime in the surface ocean here.

The changes in iron concentrations driven by a dynamic representation of ligands have the potential to further affect biological productivity, and finally thus feedback on ligand concentrations. As shown in Fig. 5 the changes in net primary production (NPP) differ much more between the two standard model runs than do the changes in iron concentration. Both models show some enhancement of NPP in the Southern Ocean, in the main coastal upwelling regions and in the subpolar gyres of the northern hemisphere. But in the Pacific, LIGA shows an increase in a narrow band along the equator through increased iron concentrations, surrounded by a decrease in NPP caused by the iron mediated increased drawdown of macronutrients in the equatorial upwelling. LIGB shows spatially more extended increase in NPP around the upwellings because production is limited here too strongly by iron. The other difference is in the Southern Indian Ocean, that changes from a super-oligotrophic (almost no primary production) to an oligotrophic system with low, but increased productivity in LIGB, while NPP actually decreases over most of the region in LIGA. The NPP increase in LIGB is probably related to the variable phytoplankton carbon:nitrogen ratio in REcoM that allows the model some production even in the strongly nitrogen-limited southern Indian Ocean (with high C:N ratio), as long as there is enough iron. As ligand production is closely tied to overall primary production, there is the potential for positive feedbacks where increased productivity due to enhanced

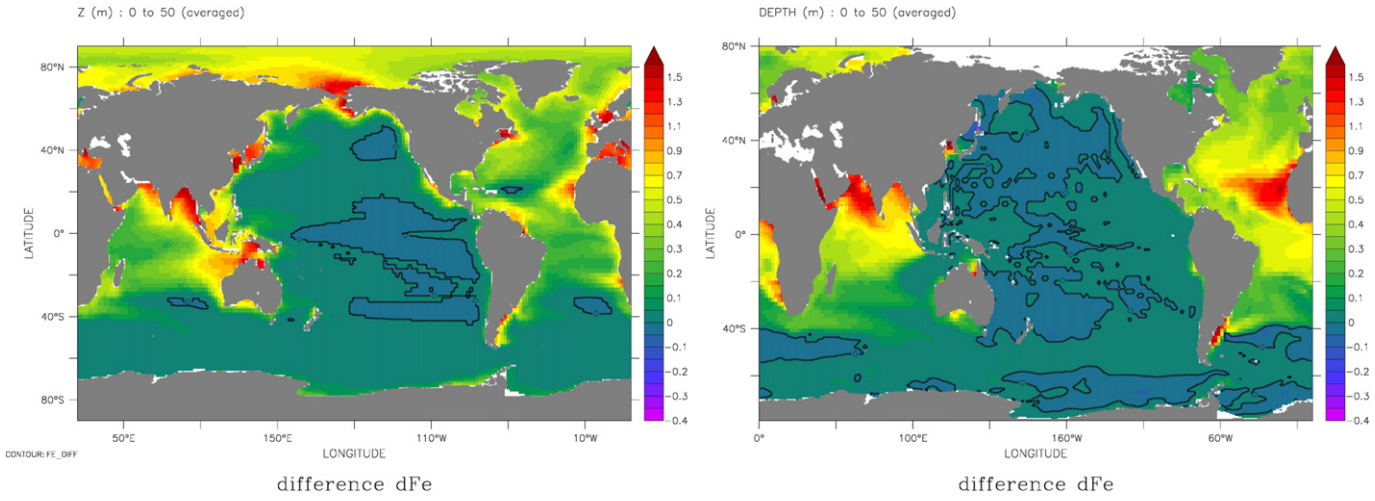

Fig. 4. Difference in surface iron concentration with and without variable ligands in model run LIGA (left), and in run LIGB (right) after 2000 years.

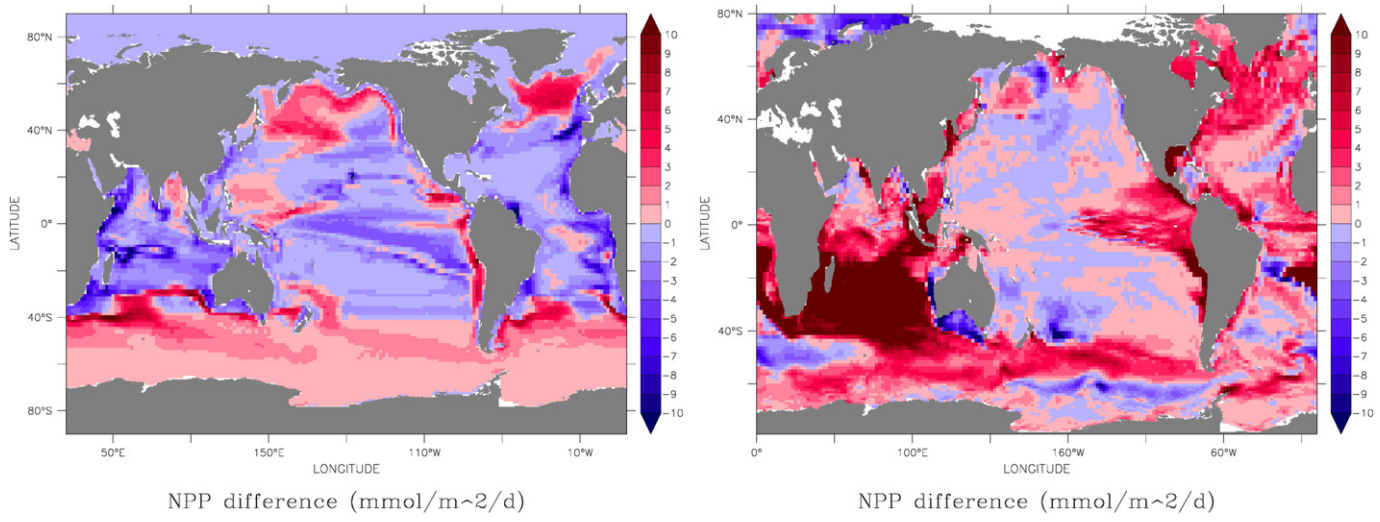

Fig. 5. Difference in net primary production betwen a run with prognostic ligands and with constant ligands. Left: run LIGA, right: run LIGB.

stabilization of dissolved iron by ligands in turn leads to higher ligand production and concentrations.

5. Sensitivities

In Section 2.2 we have presented estimates for the order of magnitude of some of the model parameters. Others, like the percentage of ligands that undergoes aggregation, are essentially unconstrained. This section presents some sensitivity runs that show how our model results depend on some of the parameter choices.

The general feature present in Fig. 6a is that increasing the photochemical degradation rate k_{phot} decreases ligand concentrations mainly in the upper ≈500 m of the water column. It is clear that the direct effect of an increased photodegradation is largest near the surface. One might have expected, however, that there is also an indirect effect on preformed ligand concentrations in deep and bottom waters. But an increased photodegradation mostly decreases ligands in the subtropical gyres, where there is little production and stable relatively shallow mixed layers, while preformed ligand concentrations in high latitudes do not change much.

Changing the fraction of ligands that undergoes aggregation p_{col} over the full range of possible values (Fig. 6b), in contrast, leads to a change in ligands over the full water depth, with the magnitude of the change, however, being larger near the surface and in the mesopelagic, and smaller in the deep ocean. This pattern is explained by the vertical decrease of particulate material and a corresponding decrease in the aggregation rate λ.

Finally, changing the ratio at which ligands are released with respect to carbon (Fig. 6c) leads to a more uniform change in the average ligand profile.

These characteristic sensitivities of the ligand profile lead to corresponding sensitivities of the iron distributions. Fig. 7 shows the covariation of globally averaged ligand and iron concentrations for the sensitivity runs. On the left we show the average over the whole water column, on the right the average over the top 50 m.

The left plot in Fig. 7 shows that — independent of which parameter we change — the change in total iron content in the ocean is tightly coupled to the change in total ligand content, with all sensitivity experiments falling nearly on one line. It is interesting to note that in the global average, iron concentrations fall below the 1:1 line, i.e. the ligand excess L_* is always positive. A similar linear relation between dissolved

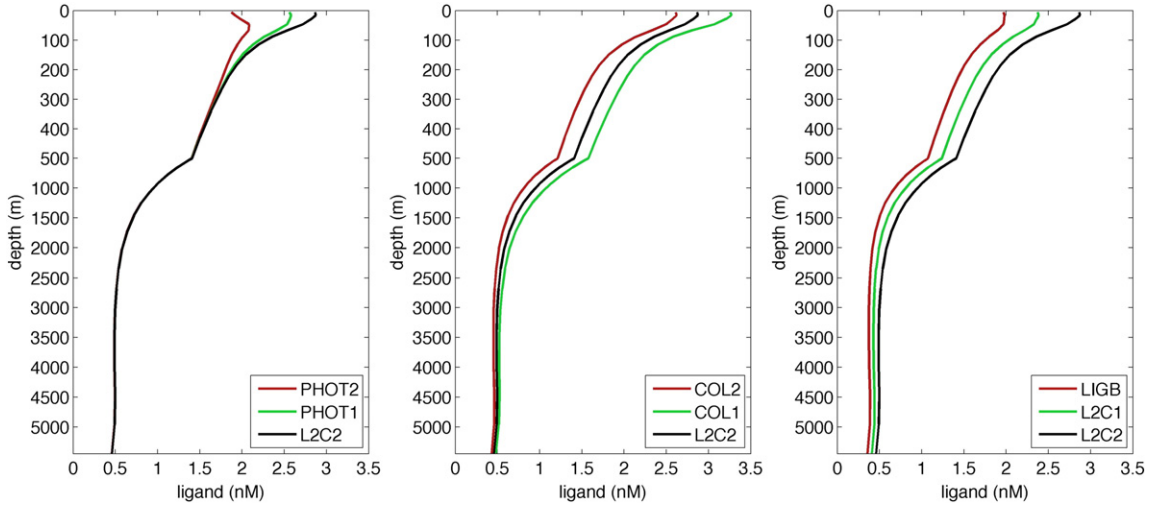

Fig. 6. Changes in the average vertical ligand profile by changing k_{phot} (left), by changing p_{col} (middle) and by changing $r_{L:C}$ (right). Note that the scaling of the depth axis is different in the upper 500 m of the water column. Ligands from run L2C2 are always shown in black.

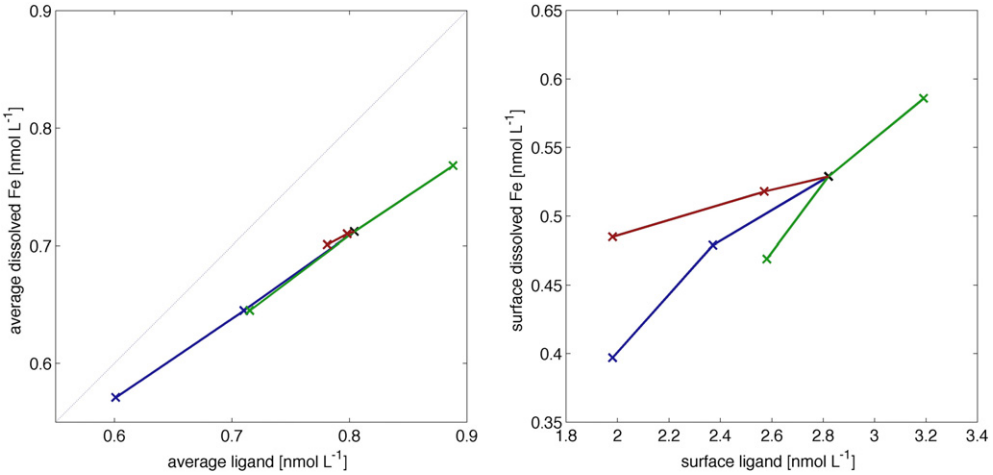

Fig. 7. Changes in globally averaged dissolved iron versus ligand concentrations for the sensitivity runs. Runs differing in $r_{L:C}$ (runs L2C2, L2C1, and LIGB) are connected by a blue line, those differing in p_{col} (runs COL1, L2C2, and COL2) by a green line, and those differing in k_{phot} (runs L2C2, PHOT1, and PHOT2) by a red line. The 'central' sensitivity run L2C2 is denoted by a black cross. The left plot shows the average over the whole water depth, the right plot the average over the top 50 m.

iron and ligands has been also found in in-situ data from the Bering Sea (Buck and Bruland, 2007). Of all the sensitivity experiment, changing the photochemical degradation rate (by a factor of 5) has the least effect on global ligand and iron concentrations, which is mostly because changes are limited to the upper ocean only.

Changes in average ligand and iron concentration near the surface (right plot in Fig. 7) are less universally coupled: While an increase in ligand always leads to an increase in iron and vice versa, the slopes of the relations are significantly different. A decrease in ligands through an increase in photochemical degradation affects ligand concentrations most strongly in the subtropical Pacific, with high mixed-layer irradiances and low production. Here iron concentrations are low anyway and decreasing ligands does not lead to further decreases. Decreasing ligand to carbon ratios, on the other hand affects ligand production everywhere, also in regions where they affect iron residence time strongly, and hence lead to a stronger iron reduction.

6. Discussion

6.1. Towards improving the modeling of ligands

The number of open-ocean observations of iron-binding ligands has steadily increased over the last decade or so, and will further do so as the international GEOTRACES program continues. One clear result of these in-situ measurements is that iron-binding ligands show substantial spatial variability in ligand concentrations between different oceanic regions (1 to 10 nM, Gledhill and Buck (2012)). In contrast, ocean biogeochemical models mostly still assume a uniform and comparatively low ligand concentration (typically between 0.6 and 1 nM). There are some exceptions to this (Tagliabue and Völker, 2011; Misumi et al., 2013), but even these newer studies rely on empirical relationships and do not attempt to describe the sources and sinks of ligands prognostically, despite the existence of a conceptual model for their dynamics (Hunter and Boyd, 2007; Ye et al., 2009).

We have made the first attempt to mechanistically model the distribution of iron-binding organic ligands in two different global OBGCMs prognostically. In both models it is possible to produce a ligand distribution that is closer to observations than a uniform low value. Moreover, the models reproduce some observed features well, such as a decrease along the conveyor belt circulation (e.g., Thuróczy et al., 2011; Mohamed et al., 2011) a general decrease of ligand concentrations from the mesopelagic towards the deep ocean (e.g., Ibisanmi et al., 2011), and a horizontally and temporally variable concentration of ligands near the surface, with higher ligands e.g. near the European shelf seas.

Both models also make strong predictions regarding the gradient in ligand concentrations between regions of high and low productivity (e.g. between upwelling regions and the subtropical gyres) that can hopefully be tested in future fieldwork. In the model at least, this gradient is strongly dependent on the assumed photochemical degradation rate. Ultimately, the predictions of the model are regulated by the sources and sinks associated with each specific process (Table 2). In this regard, process studies such as FeCycle that document the time evolution of iron–ligand dynamics (Boyd et al., 2012) can provide important information for modeling efforts. For example, the maximum rates of ligand production from organic matter remineralization reach 0.25 and 0.05 nmol L^{-1} d^{-1} in PISCES and REcoM, respectively, of similar order, but towards the low end of the two estimates of 0.3 and 1.3 nmol L^{-1} d^{-1} from Boyd et al. (2010). Further such experiments that normalize the rate of ligand production to carbon solubilization would prove invaluable. Equally so, experimental constraints on the bacterial, photochemical and aggregation losses of ligands would allow tighter constraints to be placed on these parameters.

6.2. Impact of variable ligands on dissolved iron and L_*

Modeling the ligand distribution dynamically instead of assuming a uniform and low constant concentration brings the average vertical profile of iron closer to the observed nutrient-like profile with a maximum near the oxygen minimum in the mesopelagic. However, as the ligand concentrations are now greater than those used previously, this raises the iron concentrations in the non-iron limited regions of the ocean such as the Atlantic and Indian oceans. A useful way to evaluate this effect is by looking at the excess ligand, denoted as L_* (e.g. Boyd and Tagliabue, 2015-in this issue), which is defined as: ligand minus dissolved iron. Our two models clearly overestimate the prevalence of negative L_* regions relative to that observed (Fig. 8).

The distribution of negative L_* in the models reflects external inputs of dissolved iron and highlights too low scavenging rates of uncomplexed iron. In REcoM negative L_* regions are restricted to the dust deposition regions, while in PISCES the large sedimentary iron fluxes that are absent in REcoM are also important (Fig. 7). In contrast, observational syntheses suggest that negative L_* is relatively rare (Boyd and Tagliabue, 2015-in this issue); they have been found near hydrothermal vents (Hawkes et al., 2013). While our ligand model produces an excess of ligands, relative to iron, from with DOC excretion and organic matter remineralization (i.e. positive L_*), as supported by available data (Boyd et al., 2010; Boyd

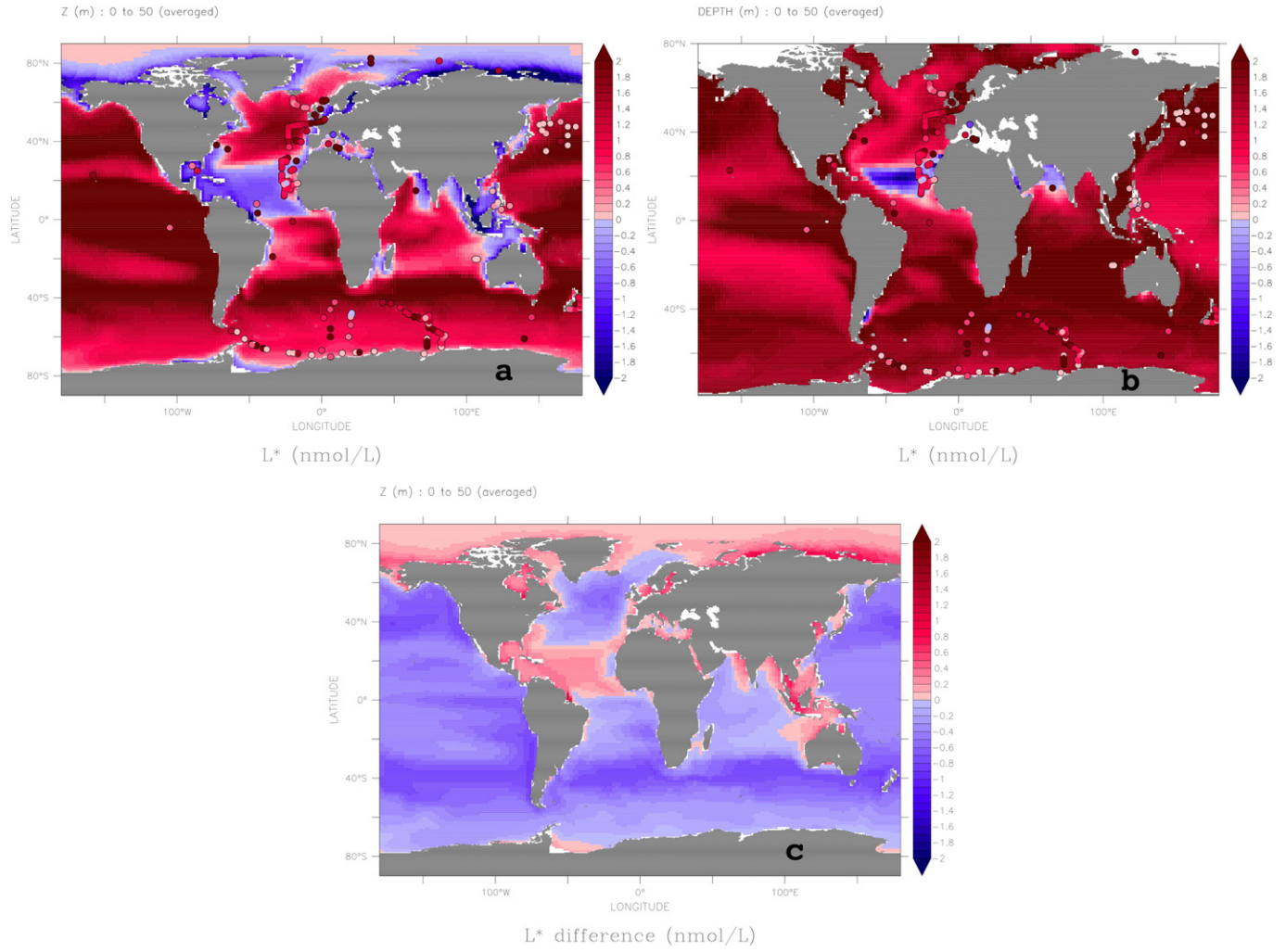

Fig. 8. Ligand excess L_* in the upper 50 m for both standard model runs (panel a: LIGA, panel b, LIGB), together with data-based estimates for this quantity (Boyd and Tagliabue, 2015-in this issue). The lower panel c shows the difference in L_* between an additional model run with changed scavenging (described in this section) and LIGA.

and Tagliabue, 2015-in this issue), neither model has external sources of ligands. Presuming dust and sediments are not expected to be sources of ligands (though Gerringa et al. (2008.) find indications for a sedimentary source of ligands), the negative L_* values we find implies that our models are able to sustain a too large fraction of uncomplexed dissolved iron (Bowie et al., 2001). This is likely a legacy of the too low and invariant ligand concentrations typically used in the past. Because of this, models needed to assume low scavenging rates to maintain iron concentrations at observed levels. Thus by increasing ligand concentrations towards measured levels, with unchanged scavenging rates, our models tend to overestimate iron. We would argue that the distribution of L_* is a powerful argument that iron biogeochemical models need a more dynamic iron cycle, with faster scavenging but also higher surface ligand concentrations.

Looking towards refining the representation of iron–ligand dynamics in ocean models, some improvement can be made by revisiting the assumptions regarding colloidal species and their cycling. As mentioned previously, our models account for colloidally associated losses of iron and ligands, but assume a fixed colloidal fraction of 0.5. If this is replaced by a dynamic colloidal fraction that is computed as a function of temperature, ionic strength and pH (Liu and Millero, 1999, 2002) and a simple doubling of the scavenging rate, the widespread increase in dissolved Fe, illustrated by L_*, associated with dynamic ligands is removed (Fig. 8c). While this indicates some improvement, it only serves to highlight that more attention should be placed on the modeling of colloidal species in future work.

6.3. Wider perspectives

The dynamism of ligand concentrations and their sensitivity to environmental variables implies the potential for significant changes in response to fluctuations in climate. For example, climate change induced changes in productivity, warming, or light intensity will affect the sources and sinks of ligands, which may then feedback onto ocean productivity via iron concentrations. At first order, we speculate that a warmer, more stratified and less productive future ocean (Bopp et al., 2013) should drive enhanced photochemical and bacterial losses of ligands, as well as reduced production rates. The reduced ligand concentrations that result may lower iron concentrations and enhance the degree of iron limitation. The relative importance of these effects remains to be tested by climate models.

The model approach presented here certainly can be improved with further insight into ligand dynamics from observations and laboratory experiments. Questions to be asked are for example: Is our parameterization of a continuum in ligand degradation rates reasonable or would it be better to model several ligand classes with different degradation rates (Hansell et al., 2012), but also possibly different photoreactivities and stability constants (Barbeau et al., 2003)? Would it be better to

make the direct production of ligands near the surface directly dependent on iron limitation of phytoplankton and/or bacteria? Are external sources of ligands, e.g. from rivers (Mikkelsen et al., 2006; Rijkenberg et al., 2006) important for the open ocean? Despite this complexity, a general paradigm for ligand cycling has emerged (Hunter and Boyd, 2007; Gledhill and Buck, 2012) that contradicts how ligands are currently simulated in OGCBMs. We have attempted to appraise how such a view can be represented in two OGCBMs and evaluate the controlling mechanisms and impact on iron cycling.

Acknowledgments

We thank Ying Ye, who started the compilation of ligand data and initiated the prognostic ligand modeling. We also thank the reviewers for their helpful and constructive comments and the Scientific Committee on Oceanic Research (SCOR) by the International Council for Science for travel support. The work of C.V. was supported by the BMBF project SOPRAN under grant agreement 03F0662C. This work made use of the facilities of N8 HPC provided and funded by the N8 consortium and EPSRC (grant EP/K000225/1) and coordinated by the Universities of Leeds and Manchester.

Appendix A. Supplementary data

Supplementary data to this article can be found online at http://dx.doi.org/10.1016/j.marchem.2014.11.008.

References

Aumont, O., Bopp, L., 2006. Globalizing results from ocean in situ iron fertilization studies. Glob. Biogeochem. Cycles 20 (2), 1–15.
Barbeau, K.A., Rue, E.L., Trick, C.G., Bruland, K.W., Butler, A., 2003. Photochemical reactivity of siderophores produced by marine heterotrophic bacteria and cyanobacteria, based on characteristic Fe(III) binding groups. Limnol. Oceanogr. 48 (3), 1069–1078.
Bopp, L., Resplandy, L., Orr, J.C., Doney, S.C., Dunne, J.P., Gehlen, M., Halloran, P., Heinze, C., Ilyina, T., Séférian, R., Tjiputra, J., Vichi, M., 2013. Multiple stressors of ocean ecosystems in the 21st century: projections with cmip5 models. Biogeosciences 10 (10), 6225–6245.
Boukhalfa, H., Crumbliss, A.L., 2002. Chemical aspects of siderophore mediated iron transport. BioMetals 15 (4), 325–339.
Bowie, A.R., Maldonado, M.T., Frew, R.D., Croot, P.L., Achterberg, E.P., Mantoura, R.C., Worsfold, P.J., Law, C.S., Boyd, P.W., 2001. The fate of added iron during a mesoscale fertilisation experiment in the Southern Ocean. Deep-Sea Res. II Top. Stud. Oceanogr. 48 (11–12), 2703–2743.
Boyd, P.W., Tagliabue, A., 2015. Using the L* concept to explore controls on the relationship between paired ligand and dissolved iron concentrations in the ocean. Mar. Chem. 173, 52–66 (in this issue).
Boyd, P.W., Ibisanmi, E., Sander, S.G., Hunter, K.A., Jackson, G.A., 2010. Remineralization of upper ocean particles: implications for iron biogeochemistry. Limnol. Oceanogr. 55 (3), 1271–1288.
Boyd, P.W., Strzepek, R.F., Chiswell, S., Chang, H., DeBruyn, J.M., Ellwood, M.J., Keenan, S., King, A.L., Maas, E.W., Nodder, S., Sander, S.G., Sutton, P., Twining, B.S., Wilhelm, S.W., Hutchins, D.a., 2012. Microbial control of diatom bloom dynamics in the open ocean. Geophys. Res. Lett. 39 (18), L18601.
Boye, M., Nishioka, J., Croot, P.L., Laan, P., Timmermans, K.R., de Baar, H.J., 2005. Major deviations of iron complexation during 22 days of a mesoscale iron enrichment in the open Southern Ocean. Mar. Chem. 96 (3–4), 257–271.
Buck, K.N., Bruland, K.W., 2007. The physicochemical speciation of dissolved iron in the Bering Sea, Alaska. Limnol. Oceanogr. 52 (5), 1800–1808.
Cullen, J.T., Bergquist, B.A., Moffett, J.W., 2006. Thermodynamic characterization of the partitioning of iron between soluble and colloidal species in the Atlantic Ocean. Mar. Chem. 98 (2–4), 295–303.
de Baar, H., de Jong, J., Bakker, D., Löscher, B., Veth, C., Bathmann, U., Smetacek, V., 1995. Importance of iron for phytoplankton spring blooms and CO_2 drawdown in the Southern Ocean. Nature 373, 412–415.
Geider, R., La Roche, J., 1994. The role of iron in phytoplankton photosynthesis and the potential for iron-limitation of primary productivity in the sea. Photosynth. Res. 39, 275–301.
Gerringa, L., Veldhuis, M., Timmermans, K., Sarthou, G., de Baar, H., 2006. Co-variance of dissolved Fe-binding ligands with phytoplankton characteristics in the canary basin. Mar. Chem. 102, 276–290.
Gerringa, L., Blain, S., Laan, P., Sarthou, G., Veldhuis, M., Brussaard, C., Viollier, E., Timmermans, K., 2008. Fe-binding dissolved organic ligands near the kerguelen archipelago in the southern ocean (Indian sector). Deep-Sea Res. II Top. Stud. Oceanogr. 55, 606–621.
Gledhill, M., Buck, K.N., 2012. The organic complexation of iron in the marine environment: a review. Front. Microbiol. 3, 69.
Gledhill, M., McCormack, P., Ussher, S.J., Achterberg, E.P., Mantoura, R.C., Worsfold, P.J., 2004. Production of siderophore type chelates by mixed bacterioplankton populations in nutrient enriched seawater incubations. Mar. Chem. 88 (1–2), 75–83.
Hansell, D.A., Carlson, C.A., Schlitzer, R., 2012. Net removal of major marine dissolved organic carbon fractions in the subsurface ocean. Glob. Biogeochem. Cycles 26 (1) (n/a–n/a).
Hassler, C.S., Schoemann, V., Nichols, C.M., Butler, E.C.V., Boyd, P.W., 2011. Saccharides enhance iron bioavailability to Southern Ocean phytoplankton. Proc. Natl. Acad. Sci. U. S. A. 108 (3), 1076–1081.
Hauck, J., Völker, C., Wang, T., Hoppema, M., Losch, M., Wolf-Gladrow, D.A., 2013. Seasonally different carbon flux changes in the Southern Ocean in response to the southern annular mode. Glob. Biogeochem. Cycles 27 (4), 1236–1245.
Hawkes, J., Connelly, D., Gledhill, M., Achterberg, E., 2013. The stabilisation and transportation of dissolved iron from high temperature hydrothermal vent systems. Earth Planet. Sci. Lett. 375, 280–290.
Hunter, K.A., Boyd, P.W., 2007. Iron-binding ligands and their role in the ocean biogeochemistry of iron. Environ. Chem. 4, 221–232.
Hutchins, D.A., Witter, A.E., Butler, A., Luther III, G.W., 1999. Competition among marine phytoplankton for different chelated iron species. Nature 400, 858–861.
Ibisanmi, E., Sander, S.G., Boyd, P.W., Bowie, A.R., Hunter, K.A., 2011. Vertical distributions of iron-(III) complexing ligands in the Southern Ocean. Deep-Sea Res. II Top. Stud. Oceanogr. 58 (21–22), 2113–2125.
Jackson, G.A., Burd, A.B., 1998. Aggregation in the marine environment. Environ. Sci. Technol. 32 (19), 2805–2814.
Kondo, Y., Takeda, S., Furuya, K., 2012. Distinct trends in dissolved Fe speciation between shallow and deep waters in the Pacific Ocean. Mar. Chem. 134–135, 18–28.
Laglera, L.M., van den Berg, C.M.G., 2009. Evidence for geochemical control of iron by humic substances in seawater. Limnol. Oceanogr. 54 (2), 610–619.
Liu, X., Millero, F.J., 1999. The solubility of iron hydroxide in sodium chloride solutions. Geochim. Cosmochim. Acta 63, 3487–3497.
Liu, X., Millero, F.J., 2002. The solubility of iron in seawater. Mar. Chem. 77 (1), 43–54.
Macrellis, H.M., Trick, C.G., Rue, E.L., Smith, G., Bruland, K.W., 2001. Collection and detection of natural iron-binding ligands from seawater. Mar. Chem. 76 (3), 175–187.
Maldonado, M.T., Price, N.M., 1999. Utilization of iron bound to strong organic ligands by plankton communities in the subarctic Pacific Ocean. Deep-Sea Res. II Top. Stud. Oceanogr. 46 (11–12), 2447–2473.
Maldonado, M.T., Price, N.M., 2001. Reduction and transport of organically bound iron by *Thalassiosira oceanica* (*Bacillariophyceae*). J. Phycol. 37 (2), 298–310.
Martin, J., Fitzwater, S., 1988. Iron deficiency limits phytoplankton growth in the northeast Pacific subarctic. Nature 331, 341–343.
Martin, J., Coale, K., Johnson, K., Fitzwater, S., Gordon, R., Tanner, S., Hunter, C., Elrod, V., Nowicki, J., Coley, T., Barber, R., Lindley, S., Watson, A., Scoy, K.V., Law, C., Liddicoat, M., Ling, R., Stanton, T., Stockel, J., Collins, C., Anderson, A., Bidigare, R., Ondrusek, M., Latasa, M., Millero, F., Lee, K., Yao, W., Zhang, J., Friedrich, G., Sakamoto, C., Chavez, F., Buck, K., Kolber, Z., Greene, R., Falkowski, P., Chisholm, S., Hoge, F., Swift, R., Yungel, J., Turner, S., Nightingale, P., Hatton, A., Liss, P., Tindale, N., 1994. Testing the iron hypothesis in ecosystems of the equatorial Pacific Ocean. Nature 371, 123–129.
Mawji, E., Gledhill, M., Milton, J.A., Tarran, G.A., Ussher, S.J., Thompson, A., Wolff, G.A., Worsfold, P.J., Achterberg, E.P., 2008. Hydroxamate siderophores: occurrence and importance in the Atlantic Ocean. Environ. Sci. Technol. 42 (23), 8675–8680.
Mikkelsen, O., van den Berg, C.M.G., Schroder, K.H., 2006. Determination of labile iron at low nmol l^{-1} levels in estuarine and coastal waters by anodic stripping voltammetry. Electroanalysis 18 (1), 35–43.
Misumi, K., Lindsay, K., Moore, J.K., Doney, S.C., Tsumune, D., Yoshida, Y., 2013. Humic substances may control dissolved iron distributions in the global ocean: implications from numerical simulations. Glob. Biogeochem. Cycles 27 (2), 450–462.
Mohamed, K.N., Steigenberger, S., Nielsdóttir, M.C., Gledhill, M., Achterberg, E.P., 2011. Dissolved iron(III) speciation in the high latitude North Atlantic Ocean. Deep-Sea Res. I 58 (11), 1049–1059.
Moore, J.K., Braucher, O., 2008. Sedimentary and mineral dust sources of dissolved iron to the world ocean. Biogeosciences 5 (3), 631–656.
Moore, C.M., Mills, M.M., Arrigo, K.R., Berman-Frank, I., Bopp, L., Boyd, P.W., Galbraith, E.D., Geider, R.J., Guieu, C., Jaccard, S.L., Jickells, T.D., La Roche, J., Lenton, T.M., Mahowald, N.M., Marañón, E., Marinov, I., Moore, J.K., Nakatsuka, T., Oschlies, A., Saito, M.A., Thingstad, T.F., Tsuda, A., Ulloa, O., 2013. Processes and patterns of oceanic nutrient limitation. Nat. Geosci. 6 (9), 701–710.
Nielsdóttir, M.C., Moore, C.M., Sanders, R., Hinz, D.J., Achterberg, E.P., 2009. Iron limitation of the postbloom phytoplankton communities in the iceland basni. Glob. Biogeochem. Cycles 23, GB3001.
Parekh, P., Follows, M.J., Boyle, E.A., 2005. Decoupling of iron and phosphate in the global ocean. Glob. Biogeochem. Cycles 19 (2).
Powell, R.T., Wilson-Finelli, A., 2003. Photochemical degradation of organic iron complexing ligands in seawater. Aquat. Sci. 65 (4), 367–374 (Dec.).
Rijkenberg, M.J.a., Gerringa, L.J.A., Velzeboer, I., Timmermans, K.R., Buma, A.G.J., de Baar, H.J.W., 2006. Iron-binding ligands in Dutch estuaries are not affected by UV induced photochemical degradation. Mar. Chem. 100 (1-2), 11–23.
Rue, E.L., Bruland, K.W., 1995. Complexation of iron(III) by natural organic ligands in the Central North Pacific as determined by a new competitive ligand equilibration/adsorptive cathodic stripping voltammetric method. Mar. Chem. 50 (1–4), 117–138.
Sato, M., Takeda, S., Furuya, K., 2007. Iron regeneration and organic iron(III)-binding ligand production during in situ zooplankton grazing experiment. Mar. Chem. 106 (3–4), 471–488.

Schartau, M., Engel, A., Schröter, J., Thoms, S., Völker, C., Wolf-Gladrow, D.A., 2007. Modelling carbon overconsumption and the formation of extracellular particulate organic carbon. Biogeosciences 4 (4), 433–454.
Schlosser, C., Croot, P.L., 2009. Controls on seawater Fe(III) solubility in the Mauritanian upwelling zone. Geophys. Res. Lett. 36 (18), 1–5.
Schlosser, C., Klar, J.K., Wake, B.D., Snow, J.T., Honey, D.J., Woodward, E.M.S., Lohan, M.C., Achterberg, E.P., Moore, C.M., 2014. Seasonal ITCZ migration dynamically controls the location of the (sub)tropical Atlantic biogeochemical divide. Proc. Natl. Acad. Sci. U. S. A. 111 (4), 1438–1442.
Shaked, Y., Kustka, A.B., Morel, F.M.M., 2005. A general kinetic model for iron acquisition by eukaryotic phytoplankton. Limnol. Oceanogr. 50 (3), 872–882.
Tagliabue, A., Völker, C., 2011. Towards accounting for dissolved iron speciation in global ocean models. Biogeosciences 8 (10), 3025–3039.
Tagliabue, A., Mtshali, T., Aumont, O., Bowie, A.R., Klunder, M.B., Roychoudhury, A., Swart, S., 2012. A global compilation of dissolved iron measurements: focus on distributions and processes in the Southern Ocean. Biogeosciences 9 (1), 1–17.
Tagliabue, A., Aumont, O., Bopp, L., 2014. The impact of different external sources of iron on the global carbon cycle. Geophys. Res. Lett. 41 (3), 920–926.
Thuróczy, C.-E., Gerringa, L.J.A., Klunder, M.B., Laan, P., de Baar, H.J.W., 2011. Observation of consistent trends in the organic complexation of dissolved iron in the Atlantic sector of the Southern Ocean. Deep-Sea Res. II Top. Stud. Oceanogr. 1–12.
Wagener, T., Pulido-Villena, E., Guieu, C., 2008. Dust iron dissolution in seawater: results from a one-year time-series in the Mediterranean Sea. Geophys. Res. Lett. 35 (16), 1–6.
Wilhelm, S.W., Trick, C.G., 1994. Iron-limited growth of cyanobacteria: multiple siderophore production is a common response. Limnol. Oceanogr. 39 (8), 1979–1984.
Wu, J., Boyle, E.A., Sunda, W.G., Wen, L.-S., 2001. Soluble and colloidal iron in the oligotrophic North Atlantic and North Pacific. Science 293 (5531), 847–849.
Ye, Y., Völker, C., Wolf-Gladrow, D.A., 2009. A model of Fe speciation and biogeochemistry at the Tropical Eastern North Atlantic Time-Series Observatory site. Biogeosciences 6 (10), 2041–2061.